Available online at www.sciencedirect.com

jmr&t Journal of Materials Research and Technology

journal homepage: www.elsevier.com/locate/jmrt

Original Article

Effect of the ausforming deformation mode on bainitic transformation in a medium carbon high silicon steel

Adriana Eres-Castellanos [a,b,c], *Muftah Zorgani* [b], *Davood Shahriari* [b,d], *Radu Romanica* [b], *Jose Antonio Jimenez* [a], *Carlos Garcia-Mateo* [a,*], *Mohammad Jahazi* [b]

[a] *National Center for Metallurgical Research (CENIM-CSIC), Avda. Gregorio del Amo 8, Madrid 28040, Spain*
[b] *École de Technologie Supérieure (ETS), Mechanical Engineering, Notre-Dame Street West, Montreal 1100, Canada*
[c] *Colorado School of Mines, Metallurgical and Materials Engineering, 920 15th St, Golden 80401, USA*
[d] *Alstom, 1251 Waterfront Place, Pittsburgh, USA*

ARTICLE INFO

Article history:
Received 7 March 2022
Accepted 5 April 2022
Available online 11 April 2022

Keywords:
Ausforming
Deformation mode
Bainitic transformation
Thermo-mechanic physical simulators

ABSTRACT

Ausforming treatments are thermomechanical treatments that consist in plastically deforming a fully austenitized steel, usually leading to either a bainitic or a martensitic microstructure. The effects of the mentioned previous deformation have been mainly studied under compression conditions. However, as widely known, many large-scale processes do not only require the application of deformation under a single mode. For that reason, it is important to assess whether different deformation modes could induce similar effects on the final microstructure. In this work, the effect of the deformation mode was analyzed in a medium carbon high silicon steel. Samples were deformed under compressive and tensile stresses at different temperatures and subsequently subjected to isothermal holding steps in the bainitic range for prolonged times. The final microstructures consisted of bainitic ferrite and retained austenite, where the bainitic ferrite was formed at different stages: a certain fraction was dynamically formed during the deformation step, while the remaining fraction was formed during the isothermal holding. The study of the changes in length observed during these treatments enabled to understand both phase transformations, while the analysis of the final microstructures by different characterization techniques, such as X-Ray Diffraction and Scanning Electron Microscopy, enabled to better understand the effect of the deformation mode at different levels. It was proved that tensile ausforming led to more rapid and intense strain induced transformations than compression ausforming. Moreover, results showed that ausforming led to anisotropic structures, regardless of the deformation mode, where bainitic ferrite plates were aligned with respect to the deformation direction. The effect of the deformation mode on the bainitic ferrite plate thickness, the volume fractions of the different phases, several crystallographic parameters and hardness is also discussed.

* Corresponding author.
E-mail address: cgm@cenim.csic.es (C. Garcia-Mateo).
https://doi.org/10.1016/j.jmrt.2022.04.033

1. Introduction

Most of the industrial processes involve deformation, with the aim of leading to a given part geometry and, at the same time, attaining a desired microstructure with optimal mechanical properties. In this sense, ausforming treatments are thermomechanical treatments that consist in plastically deforming a fully austenitized steel below the recrystallization stop temperature and before a displacive transformation takes place [1]. This treatment has been envisioned as a way to improve the mechanical response of the attained microstructure, as well as the resultant microstructural characteristics and the phase transformation kinetics [2]. Regarding the effect of ausforming on the bainitic transformation, some of the conclusions that have been made so far, based on studies that use a compressive deformation mode, are: (a) ausforming refines the final bainitic microstructure under certain conditions [3], (b) the application of deformation prior to the bainitic transformation can stabilize the secondary phase – austenite - against any displacive transformation [4,5]; (c) ausforming promotes the nucleation of bainitic ferrite, i.e. kinetics are accelerated [6] and (d) ausforming can lead to variant selection phenomena, i.e. only few crystallographic bainitic ferrite variants are selected, which makes the bainitic transformation deformation anisotropic [7,8] and the final bainitic microstructure highly aligned [8] along microbands formed in the austenite during the deformation step [9].

Although ausforming has been mainly studied under compression conditions [8,10,11], many metal forming processes - such as rolling, forging or extrusion - are associated to the application of deformation under several deformation modes. Parts are usually subjected to complex deformation states, where some regions may be compressed, while other regions may undergo tension. For that reason, it is important to assess whether different deformation modes could induce similar microstructural effects. The differences between the application of a compression and a tensile deformation, during ausforming treatments, in terms of the final microstructure, have, for instance, barely been studied. To the authors' knowledge, only Chen et al. [12] addressed the effect of the deformation mode on the bainitic transformation during ausforming treatments. To do so, they used a medium carbon high silicon steel, their deformation temperatures were in the range 800–1000 °C and their isothermal temperature was 350 °C. However, they mainly focused on the kinetics of the transformation, concluding that compression deformation accelerates the formation of bainite, while tensile deformation delays it.

In this work, the effect of the deformation mode (compression vs. tension) has been studied by performing the same ausforming treatments in different thermomechanical simulators. The deformation temperatures were always close or lower than the bainite start temperature. Because of the technical differences between the thermo-mechanic physical simulators used to apply each deformation mode, i.e. Bähr 805D dilatometer and Gleeble™ 3800, several machine parameters had to be optimized by using a set of preliminary tests. Subsequently, the phase transformations happening during the whole thermomechanical treatments were analyzed as a function of the deformation mode by analyzing the changes in length during the tests and, finally, the obtained microstructures were characterized and compared by different techniques, such as Scanning Electron Microscopy (SEM), X-Ray Diffraction (XRD) and hardness measurements.

2. Experimental

In this work, the commercial steel SCM40, manufactured by Sidenor and containing 0.4 wt % C and 3 wt % Si, among other alloying elements, was subjected to thermal and thermomechanical treatments by using a Bähr 805D high-resolution dilatometer and a Gleeble™ 3800 thermomechanical simulator. This steel had been hot rolled and globularized. Dilatometry samples were cylinders of 10 mm length and 4 or 5 mm diameter, where the highest diameter was used when compressive deformation was applied. Gleeble™ 3800 samples were cylinders of 6 mm diameter and 127 mm length, where the two ends of the sample were threaded (15.25 mm in each side) to be fixed to the grips of the simulator.

In both equipment, purely thermal tests (without deformation) and thermomechanical treatments (under compression/tension) were performed, where the thermal treatments were used as a reference. Fig. 1 includes sketches of the set ups used to perform both thermal and thermomechanical treatments in the Bähr 805D dilatometer and in the Gleeble™ 3800 simulator. To heat the samples, the Bähr 805D dilatometer was equipped with an induction heating coil, while samples were heated up in the Gleeble™ 3800 by resistive heating. A helium quenching system was available to use in the Bähr 805D dilatometer, whereas no quenching system was used for the Gleeble™ 3800 tests due to reasons that are given later on. However, the jaws to which the grips holding the samples are attached in the Gleeble™ 3800 were water-cooled during the whole experiment, to prevent the equipment from being affected by the high temperature. In both cases, the temperature was controlled by a type K thermocouple welded to the central part of the sample surface. In addition, in some cases, extra thermocouples were welded to the Gleeble™ 3800 samples at different distances from the center to study the thermal gradient over the specimen. The repeatability and reliability of the experiments was confirmed by previous studies, where several tests were run, proving to lead to very similar results.

In addition, both simulators enabled to measure the changes in length along the samples during the tests to study the phase transformations taking place. The Bähr 805D dilatometer uses a Linear Velocity Displacement Transducer (LVDT) to measure the dimension change. In the case of the thermal tests, the LVDT is connected to fused silica pushrods, while, in the case of the compression tests, it is connected to a deformation module with silicon nitride punchers. The punchers were separated from the samples by molybdenum films to reduce friction [13,14]. The Gleeble™ 3800 also uses a lengthwise LVDT strain gauge that detects the changes in length of the whole sample, not only to its central part, where the temperature equals the programmed one. For that reason, the use of a full bridge strain gauge type hot zone transducer (HZT-072) with alumina rods was necessary. The HZT-072 had

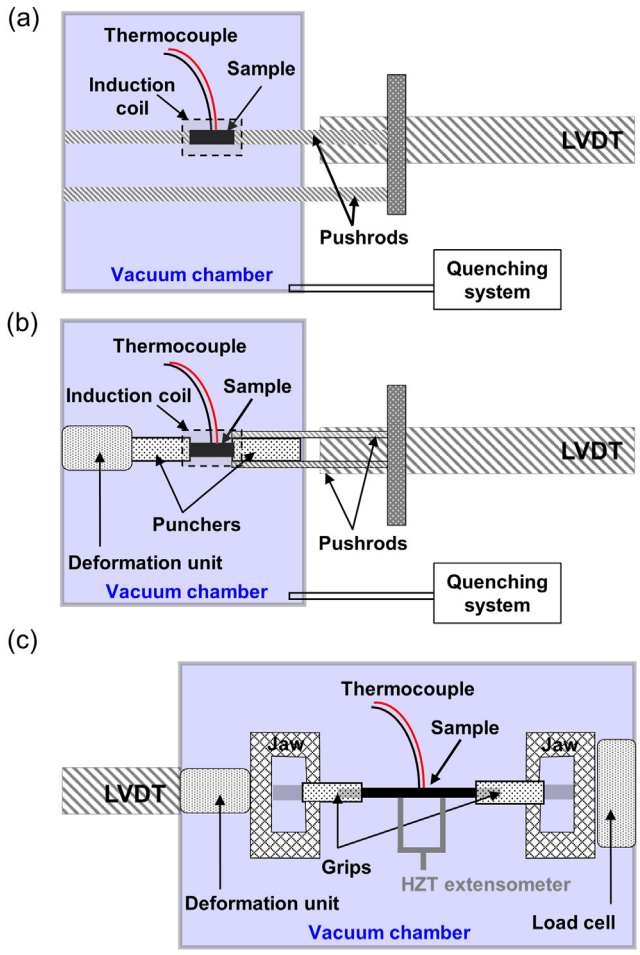

Fig. 1 – Sketch of the set up used for: (a) thermal tests performed in Bähr 805D dilatometer; (b) thermomechanical tests performed in Bähr 805D dilatometer and (c) thermal and thermomechanical tests performed in Gleeble™ 3800 thermomechanical simulator.

a gauge length of 25 mm. Travel distance for this type of extensometer is 12.5 mm and 5 mm in tension and compression, respectively. The initial distance between the HZT-072 extensometer rods was set to 20 mm, as later discussed. All the strain and strain rate values reported for the Gleeble™ 3800 therefore correspond to the ones measured with the HZT-072.

Specimens were subjected to the same thermal and thermomechanical treatments that were performed in a previous work [15], i.e. several ausforming treatments and a reference pure isothermal treatment, whose sketches are shown in Fig. 2. Firstly, samples were heated up to 990 °C at a heating rate of 5 °C/s and held during 4 min to ensure fully austenitization. Subsequently, the reference sample was cooled down to an isothermal holding temperature lying in the bainitic range, T_{ISO}, which was selected as 350 °C. The sample was held for 1 h at this temperature (isothermal time, t_{ISO}), which is long enough for the completion of the bainitic transformation. The cooling rate was set as 15 °C/s in the Bähr 805D dilatometer for the specimens with and without ausforming, whereas the cooling rate achieved in the Gleeble™ 3800 thermomechanical simulator was not constant and equal to or less than 5 °C/s, as explained in next section. In the case of the ausforming treatments, after austenitization, samples were cooled down to the deformation temperature T_{DEF} keeping the same corresponding cooling rates. Two T_{DEF} were selected, i.e. 520 °C (in the hiatus between the bainitic and the ferritic/pearlitic regions [8]) and 400 °C (in the bainitic domain). In the Bähr 805D dilatometer, the samples were deformed under compression to an engineering strain of 0.1 with a strain rate of 0.04 s^{-1}, while in the Gleeble™ 3800 thermomechanical simulator, similar deformation was performed under uniaxial tensile loading at the same strain rate. Soaking times of 15 and 10 s before and after the deformation step were included to let the sample temperature homogenize and to enable for the sample elastic recovery, respectively. After deformation, samples were cooled to T_{ISO}, and held for 1 h at this temperature before cooling to room temperature at 25 °C/s and <1 °C/s in the Bähr 805D and in the Gleeble™, respectively.

The microstructures were characterized on the transverse (T) and longitudinal (L) sections of the sample center by optical microscopy (OM) and by a JEOL JSM-6500 field emission gun (FEG) - SEM operating at 10 kV. To do so, standard

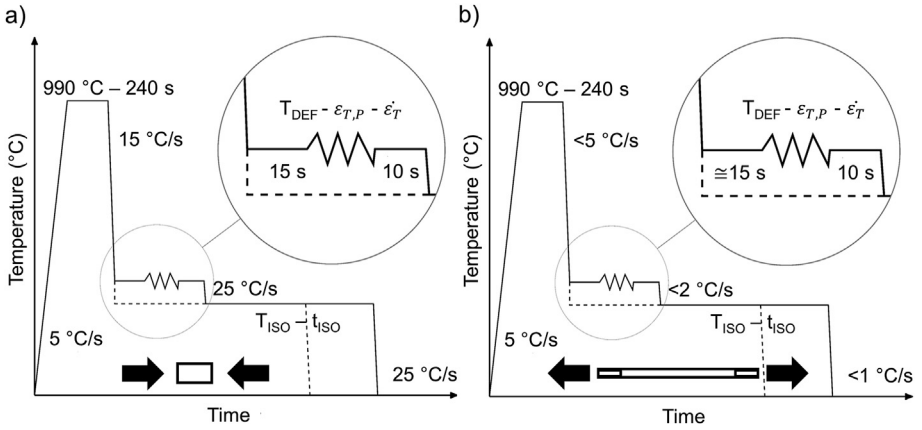

Fig. 2 – Sketch of the thermal (dashed line) and thermomechanical (continuous line) treatments using: (a) a Bähr 805D dilatometer and (b) Gleeble™ 3800 simulator. T_{DEF}, T_{ISO}, t_{ISO}, $\varepsilon_{T,P}$ and $\dot{\varepsilon}_T$ stand for deformation temperature, isothermal temperature, isothermal time, true plastic strain and strain rate, respectively.

metallographic procedures were used, including grinding, polishing and revealing the microstructure using a Nital 2% solution. The SEM micrographs were used to measure the bainitic ferrite plate thickness on both sections by following the procedure explained in Ref. [16], which consists in manually measuring linear intercepts perpendicularly to the bainitic ferrite plates on SEM micrographs and subjecting their average value to a stereographic correction. For this work, 500 measurements were made per condition. Results are always followed by their corresponding 95% confidence error. Moreover, the angle between ~ 500 plates per condition and the deformation direction (DD) were measured on SEM micrographs of the L sections.

The microstructures were also characterized by X-Ray Diffraction (XRD), for which they were metallographically prepared as previously described. It must be emphasized that, the standard preparation procedure was followed by several etching and polishing cycles to avoid the presence of martensite induced by deformation during the grinding and polishing steps. XRD measurements were performed by a Bruker AXS D8 X-ray diffractometer, equipped with a Goebel mirror for parallel-beam geometry and a LynxEye Linear Position Sensitive Detector. Conventional diffraction patterns were collected in Bragg–Brentano geometry using Co radiation ($\lambda = 1.789$ Å), over a 2θ range of 45–135°, with a step size of 0.01°. It has been reported elsewhere that the Rietveld refinement is a suitable approach for quantifying and calculating structural parameters of crystalline phases from XRD patterns. It should be noted that the microstructure of high silicon content medium carbon steels is characterized by the presence of tetragonal bainitic ferrite [17] and retained austenite with both blocky and thin film morphology. Since the thin film-type of austenite is characterized by a higher C content in solid solution and a much smaller crystallite size, the peaks of austenite show asymmetry in the recorded diffraction spectra. Once the peak asymmetry due to axial divergence was eliminated by using Soller slits and the instrument functions determined from the profile shape analysis of a corundum sample measured under the same conditions, each of the austenite diffraction peaks can be deconvolved into two peaks, which correspond to a carbon poor (γ^{+}) and carbon rich (γ^{++}) austenite. Then, Rietveld refinements were performed using as starting points the structure for the body centered tetragonal ferrite and two austenite like structures with a close lattice parameter. Line broadening effects were analyzed with the double-Voigt approach [15] and the spherical harmonics modeling was used to correct the texture effect. The refined parameters included the lattice parameters of these three phases, their crystallite size (λ) and the micro-strain (ε). From the austenite lattice parameter and the bulk chemical composition, the corresponding carbon content can be calculated using the equation proposed by Dyson and Holmes:

$$a_{\gamma} = 3.578 + 0.033\,w_C + 0.00095\,w_{Mn} - 0.0002\,w_{Ni} + 0.0006\,w_{Cr} + 0.022\,w_N + 0.0056\,w_{Al} - 0.0004\,w_{Co} + 0.0015\,w_{Cu} + 0.0031\,w_{Mo} + 0.0051 w_{Nb} + 0.0039\,w_{Ti} + 0.0018\,w_V + 0.0018\,w_W$$

where w_i is the weight percent of the element i [18]. Moreover, the carbon content of bainitic ferrite can also be calculated from its lattice parameters, considering the effects of carbon content on cell tetragonality according to Cohen's equation: $c_{\alpha_B}/a_{\alpha_B} = 1 + 0.045 w_C$ [19]. Finally, the dislocation density of the bainitic ferrite (ρ_{α_B}) was calculated as a function of the crystallite size and the micro-strain by the relationship proposed by Williamson and Smallman, i.e. $\rho_{\alpha_B} = (3k_{\alpha_B}\varepsilon^3_{\alpha_B}/Fb^2_{\alpha_B}\lambda^2_{\alpha_B})^{0.5}$, where k_{α_B} is a constant that equals 14.4, b is the magnitude of the Burger's vector (assumed as 0.258 nm) and $F = 1$ [20]. All the reported errors have been calculated by error propagation, considering that the errors of the volume fraction, the lattice parameter, the crystallite size and the micro-strain are 3%, 0.001 Å, 2 nm and $2 \cdot 10^{-4}$, respectively. On the other hand, it is very likely that the results obtained for crystallite size and microstrain present a limited reliability characterized by a larger error and associated with a large standard deviation.

Hardness measurements were made on polished samples, subjected to standard metallography preparation. Rockwell A hardness (HRA) was measured to build hardness profiles along the Gleeble™ 3800 samples, where the measurements were made on the sample surface and on the sample core. In the former case, values had to be corrected to account for the curvature of the sample surface, according to ASTM E18-20. Additionally, Rockwell C hardness (HRC) and Vickers hardness (HV) were measured on the central T section of both Bähr 805D dilatometer and Gleeble™ 3800 samples. The reported values correspond to the average of at least 3 measurements, accompanied by its standard deviation.

Finally, crystallographic theoretical calculations were performed in Matlab®, by using its toolbox MTEX [21].

3. Results and discussion

3.1. *As received material, design of thermal and thermomechanical treatments and microstructural gradient*

As previously mentioned, samples were machined (to the previously described dimensions) from bars made out of the Sidenor's commercial steel SCM40, which had been hot-rolled and globularized. Its hardness was 61.3 ± 0.9 HRA/22.0 ± 3.9 HRC.

Specimens were subjected to the treatments described in Section Experimental. The design of the thermal and thermomechanical treatments performed in the Bähr 805D dilatometer was rather straightforward, as the piece of equipment enabled a perfect control of the deformation and the temperature. The achieved true plastic strains ($\varepsilon_{T,P}$), strain rates ($\dot{\varepsilon_T}$) and maximum true stresses (σ_{T-max}) are reported in Table 1. It is noteworthy to mention that the deformation was non-uniformly distributed during the thermomechanical compression treatments, forming an X-shaped pattern, where the deformation was uniaxial and maximum at the sample center [9].

Due to the particularities associated to the Gleeble™ 3800 thermomechanical simulator and the geometry and dimensions of the samples, certain modifications had to be

Table 1 – True plastic strain and strain rate achieved during the Bähr 805D dilatometer and Gleeble™ 3800 tests. $\varepsilon_{T,P}$ and $\dot{\varepsilon_T}$ stand for true plastic strain and strain rate, respectively.

Condition	Equipment	$\varepsilon_{T,P}$	$\dot{\varepsilon_T}$ (s^{-1})	σ_{T-max} (MPa)
T_{DEF} = 520 °C, T_{ISO} = 350 °C	Bähr 805D	0.0980	0.0335	416
	Gleeble™ 3800	0.0795	0.0268	390
T_{DEF} = 400 °C, T_{ISO} = 350 °C	Bähr 805D	0.0951	0.0322	461
	Gleeble™ 3800	0.0894	0.0298	446

made. The main differences of the Gleeble™ 3800 simulator, as compared to the Bähr 805D dilatometer, were related to the achievable cooling rates, the thermal gradients and the distribution of deformation along the samples. Whereas the Bähr 805D dilatometer was equipped with a quenching system, using the Gleeble™ 3800 quenching system proved to lead to significant oxidation problems on the sample surface, reason why it was decided to dispense with it. Regarding the temperature distribution, as the grips to which the Gleeble™ 3800 samples were fixed were refrigerated by water, there was a temperature gradient from the sample center to the two ends of the sample. Finally, the distribution of the strain along the tensile samples was unknown. To assess how to obtain the same thermal and deformation conditions in both thermomechanical simulators, several trial tests were carried out, as detailed below.

To study the achievable cooling rates and the thermal gradient, an austenitization (at 990 °C for 4 min) and cooling treatment was performed. The aim of this treatment was to analyze the maximum cooling rates that could be achieved by the Gleeble™ 3800 simulator. Furthermore, heat-treated, several thermocouples were welded to the sample - 5, 10, 20 and 30 mm away from its center - to study the thermal gradient along the sample. A sketch showing the position of the thermocouples during the experiment is shown in Fig. 3. Fig. 3 also shows the evolution of the temperature (Fig. 3(a)a) and heating/cooling rate (Fig. 3(b)) as a function of the time, as well as the maximum absolute temperature difference detected by four thermocouples welded along the length of the sample (Fig. 3(c)) for the above described treatment. Data corresponding to the thermocouple welded at 20 mm from the sample center stopped being recorded during the austenitization step since the thermocouple got detached. For the rest of the thermocouples, data stopped being recorded below 300 °C.

As can be observed in Fig. 3(a, b), from the sample center to 10 mm away from it, the heating and austenitization steps were very similar to the ones obtained by dilatometry. The maximum obtained cooling rate was 5 °C/s, still high enough to be above the critical cooling rate (estimated to be below 2 °C/s by a complementary dilatometry study). However, the cooling rate of 5 °C/s was only well achieved until the temperature was approximately 500 °C. From that temperature down, the programmed cooling rate was not achieved anymore and, as the temperature decreased, so did the absolute value of the cooling rate. The behavior was very different 20 and 30 mm away from the sample center, where the austenitization temperature was never reached, see

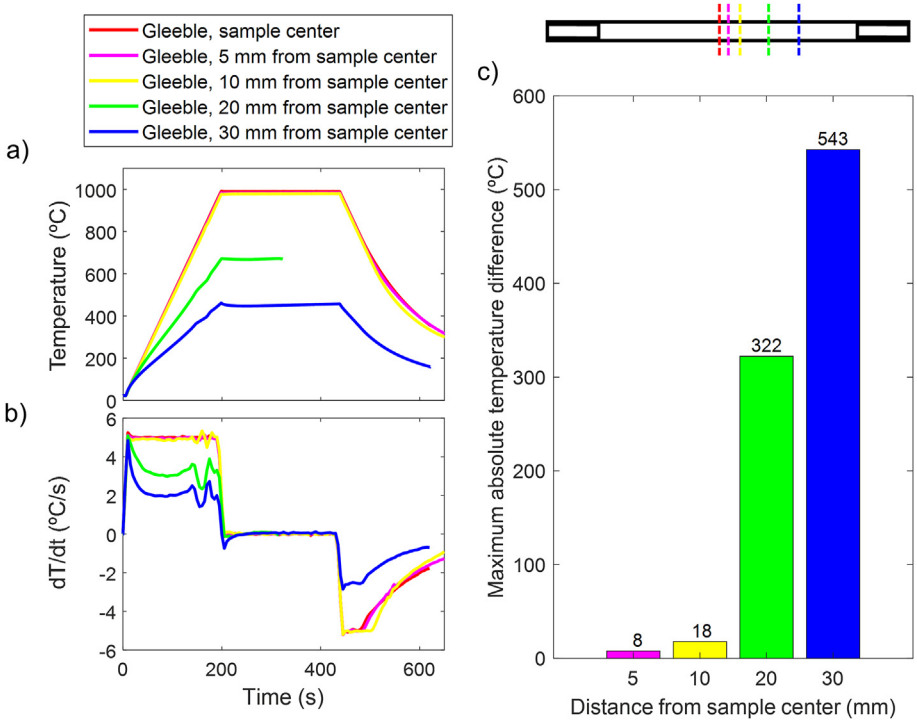

Fig. 3 – (a) Temperature – time and (b) dT/dt (heating or cooling rate)–time plots obtained by the Gleeble™ 3800 simulator at several distances from the sample center; (c) maximum absolute temperature difference between the corresponding point, which lies at several distances from the sample center, and the sample center. The sketch on the top right part shows where thermocouples were welded.

Fig. 3(a, b), and the maximum absolute temperature change was 322 and 543 °C, respectively. The steel critical temperatures Ac1 and Ac3 (experimentally determined by dilatometry) were 842 and 961 °C, which meant that the sample was austenitized in neither region. Therefore, during the subsequent Gleeble™ 3800 tests, it was considered that the samples presented a microstructural gradient from the as-received microstructure (in regions that were not austenitized, close to the threads) to a mixture of the as-received microstructure and a bainitic microstructure (in regions that were partially austenitized) and to a fully bainitic microstructure (in the central 20 mm of the samples, that were fully austenitized).

Although the previous experiments confirmed that the microstructure became fully bainitic along the central 20 mm of the samples, it was decided to place the HZT-072 extensometer rods 10 mm apart from the sample center to minimize the thermal gradient. However, it was un-known whether such a distance was low enough to lead to a uniform deformation in that region during the ausforming treatments. To study so, an extra test was conducted. Before carrying out the test, three couples of marks were made on the sample surface, at different distances from the sample center, where the furthest marks were separated by 25.6 ± 0.1 mm from each other. The distances between each couple of marks can be seen in Table 2. The sample was subjected to an ausforming treatment, such as the one in Fig. 2(b), where $T_{DEF} = 520$ °C, $T_{ISO} = 300$ °C, $t_{ISO} = 5$ min, $\varepsilon_{T,P} = 0.1164$ and $\dot{\varepsilon}_T = 0.0536\ s^{-1}$. Note that the last two values were calculated from the HZT-072 extensometer data after the test. After the test took place, the distance between the marks was re-measured. Considering that the thermal gradient was small enough not to significantly affect the phase transformations during the thermomechanical treatment, the only reason that would explain variations in the strain would be that the deformation was not uniform. Table 2 includes the final distances between the three couples of marks, in addition to their corresponding $\varepsilon_{T,P}$ values, calculated from the initial and final distances. As can be observed, considering the errors, the $\varepsilon_{T,P}$ values were very similar. Hence, it was assumed that the deformation was uniform along the central 25 mm of the samples.

In summary, the carried-out trial tests enabled to conclude that the temperature and strain distributions were uniform along the central 20 mm of the Gleeble™ 3800 samples, where the HZT-072 extensometer rods were placed. In this way, it was made sure that these sample regions, delimited by the extensometer rods, were subjected to the same thermal and thermomechanical treatments as the dilatometry samples, and therefore the strains and strain rates achieved by tensile tests were similar to the ones obtained by dilatometry (compression mode). To do so, several tests with different strain and strain rate values were run with the Gleeble™ 3800 until the obtained true plastic strains and strain rates were comparable to the Bähr 805D dilatometer ones. The schematic diagrams of the designed ausforming treatments to be performed in the Gleeble™ 3800 thermomechanical simulator are included in Fig. 2. The achieved true plastic strains and strain rates, according to the data recorded by the HZT-072 extensometer, are reported in Table 1, together with the maximum true stresses. As can be observed, the maximum true stress values obtained for different deformation modes are comparable.

Table 2 – Initial and final distances between couples of marks drawn on the sample surface of the ausforming treatment performed to study the distribution of the deformation along the central part of the samples and the corresponding true plastic strain values, $\varepsilon_{T,P}$.

	Marks 1	Marks 2	Marks 3
Initial distance (mm)	12.5 ± 0.1	20.4 ± 0.1	25.6 ± 0.1
Final distance (mm)	14.0 ± 0.1	23.0 ± 0.1	28.8 ± 0.1
$\varepsilon_{T,P}$	0.1131 ± 0.016	0.1206 ± 0.026	0.1180 ± 0.032

The microstructural gradient along the samples subjected to the designed treatments in the Gleeble™ 3800 was studied by the hardness measurements (HRA) that can be observed in Fig. 4, where they are compared to the HRA value of the as-received microstructure. As expected, the hardness values were much higher in the central 20 mm of the samples, where the HRA values slightly decreased close to the sample center. This is probably because of the reported low thermal gradient in region (18 °C according to Fig. 3(c)), which could have affected the volume fraction of bainitic ferrite. However, it can be assumed that this microstructural gradient was not very significant. As the distance from the center is further increased, the hardness decreased until it equaled the hardness of the as-received microstructure. As can be seen, the hardness values were always slightly lower in the core than at the surface, which is most likely due to the fact that samples are cooled down faster on their surface than on their core, affecting their microstructure. This phenomenon has been reported in Gleeble™ experiments in the past [22]. Based on these results, it was decided to only further characterize the Gleeble™ 3800 samples on their center, on both T and L sections.

3.2. *Characterization of the phase transformations and the resultant microstructures in the samples center*

The analysis of the data obtained by the thermocouples, the LVDT sensor (in Bähr 805D) and the HZT-072 extensometer (in Gleeble™ 3800) enabled to understand the phase transformations taking place during the thermal and thermomechanical treatments in the samples center. Fig. 5 includes the temperature – time and relative change in length–time plots corresponding to the whole treatment and to the isothermal holding at 350 °C, respectively.

For the isothermal treatments, the information obtained during the whole treatment was comparable, regardless of the equipment in which they were performed. As can be seen in Fig. 5(d), the bainitic phase transformations in both simulators were very similar in terms of kinetics and maximum relative change in length.

Data corresponding to the ausforming treatments showed differences depending on the deformation temperature and the deformation mode. In the case of the ausforming treatment with $T_{DEF} = 520$ °C, there were no significant differences during the whole treatment until the deformation step was finished. However, the signal obtained during the isothermal

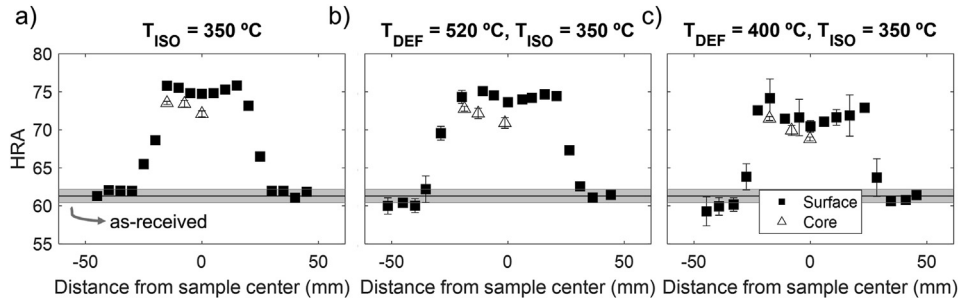

Fig. 4 – HRA profiles corresponding to the samples subjected to (a) an isothermal treatment at 350 °C; (b) an ausforming treatment at 520 °C and (c) an ausforming treatment at 400 °C in the Gleeble™ 3800 thermomechanical simulator. The squares and triangles correspond to the surface and the core hardness measurements, respectively, and the shadowed horizontal area corresponds to the hardness value of the as-received microstructure.

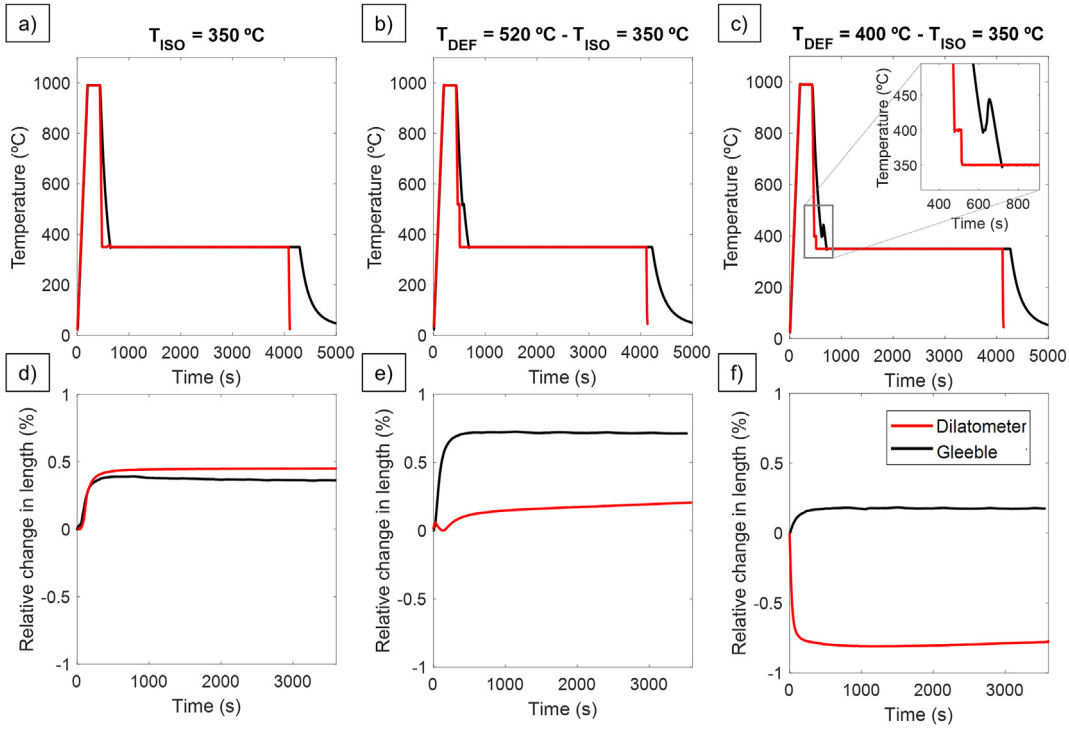

Fig. 5 – Temperature–time plots during the whole treatment (a–c) and relative change in length–time plots during the isothermal holding at 350 °C (d–f). Plots correspond to the samples subjected to (a, d) an isothermal treatment at 350 °C; (b, e) an ausforming treatment at 520 °C and (c, f) an ausforming treatment at 400 °C in both the Bähr 805D dilatometer and the Gleeble™ 3800.

holding at 350 °C for the tension ausforming test T_{DEF} = 520 °C was very different to the one obtained for the compression ausforming test, see Fig. 5(e). While the compression sample showed a maximum relative change in length lower than the one obtained for the reference isothermal treatment, in good agreement with previous results [8], the maximum relative change in length corresponding to the tension sample was higher than that of the isothermal treatment (Fig. 5(d) vs. Fig. 5(e)). This behavior is probably due to a variant selection phenomenon, as the application of deformation and the formation of deformation micro-bands in the prior austenite [23] has been previously shown to affect the anisotropy of the transformation during ausforming treatments [7]. The above results suggest that the modification of the deformation mode from compression to tensile, affects the distribution of the deformation micro-bands, which most likely alters the way in which anisotropy is affected. The above dilatometric results are also consistent with the results obtained on isothermally treated samples under constant stresses. Whereas several authors reported that constant tensile stresses would increase the length change along the Z-axis (and decrease the dilatometric intensities along the radial axes) [24,25], the opposite behavior has been found in samples subjected to isothermal treatments under compressive stresses [26].

The change in the deformation mode did not affect the austenitic structure, but also the formation of strain induced

bainitic ferrite during the deformation step for the ausforming condition with $T_{DEF} = 400$ °C, see Fig. 5(c, f). A previous study [15], where the same compression ausforming treatments were performed to the same steel, revealed the formation of small fractions of strain induced bainitic ferrite after compressing the austenite by 10% at 400 °C, caused by the increase of driving force because of the application of high stresses. For the experiments of study, the maximum true stresses attained at 400 °C and reported in Table 1 were very similar, regardless of the deformation mode, suggesting at first that a similar fraction of strain induced bainitic ferrite was formed under tension. Note that the formation of strain induced bainite leads to a stress increase, reason why these values can be used as an indicative of the presence of these metastable phases. However, one can observe a temperature increase of ~ 50 °C detected during and after the deformation step in the sample subjected to tensile ausforming at 400 °C, see Fig. 5(c). A possible reason of why temperature increases at this stage could be the formation of a very high fraction of bainitic ferrite at this temperature, as the bainitic transformation is exothermic [27]. Although further in-situ experimental evidence or complementary experiments would enable to definitely prove the presence of these metastable phases formed due to the application of stress, the authors can offer different arguments of why they think strain induced bainitic ferrite formed in a higher extent under the application of tensile deformation. In first place, previous studies on austenitic stainless steels have proven that subjecting the prior austenite to tensile deformation promotes the formation of strain induced displacive phases in a higher extent than a compressive deformation [28]. Secondly, these experimental results are in good agreement with the theory by Patel and Cohen, who proposed an equation for the mechanical driving force introduced by an applied stress in a given austenitic structure (ΔG_{mech}), where the equation led to higher absolute values if the deformation mode was tension [29]. Moreover, the temperature increase would also lower the attained stress levels for this condition, explaining why the maximum stress values were similar, regardless of the deformation mode. Finally, the observed relative change in length signals present in Fig. 5(f) can also help to indirectly prove the formation of strain induced bainitic ferrite. It can be observed that the relative change in length values obtained during tensile ausforming are lower than the ones reported for tensile ausforming at $T_{DEF} = 520$ °C - Fig. 5(e). While compression ausforming is expected to lead to more negative signals as the deformation temperature decreases [7], the dilatometric signal obtained during tensile ausforming should be positive and higher than the one obtained for the ausforming treatment at 520 °C [24,25]. However, this signal is even lower than the one obtained in the absence of deformation, see Fig. 5(f vs. d). This behavior can be explained by the presence of a high-volume fraction of strain induced bainitic ferrite during tensile ausforming, which would lower the amount of austenite available to transform at 350 °C, during the isothermal holding.

Further characterization by SEM observation, HRC measurements and XRD analyses enabled to understand the product of the discussed phase transformations. Fig. 6 and Fig. 7 show OM and SEM transverse (T) and longitudinal (L)

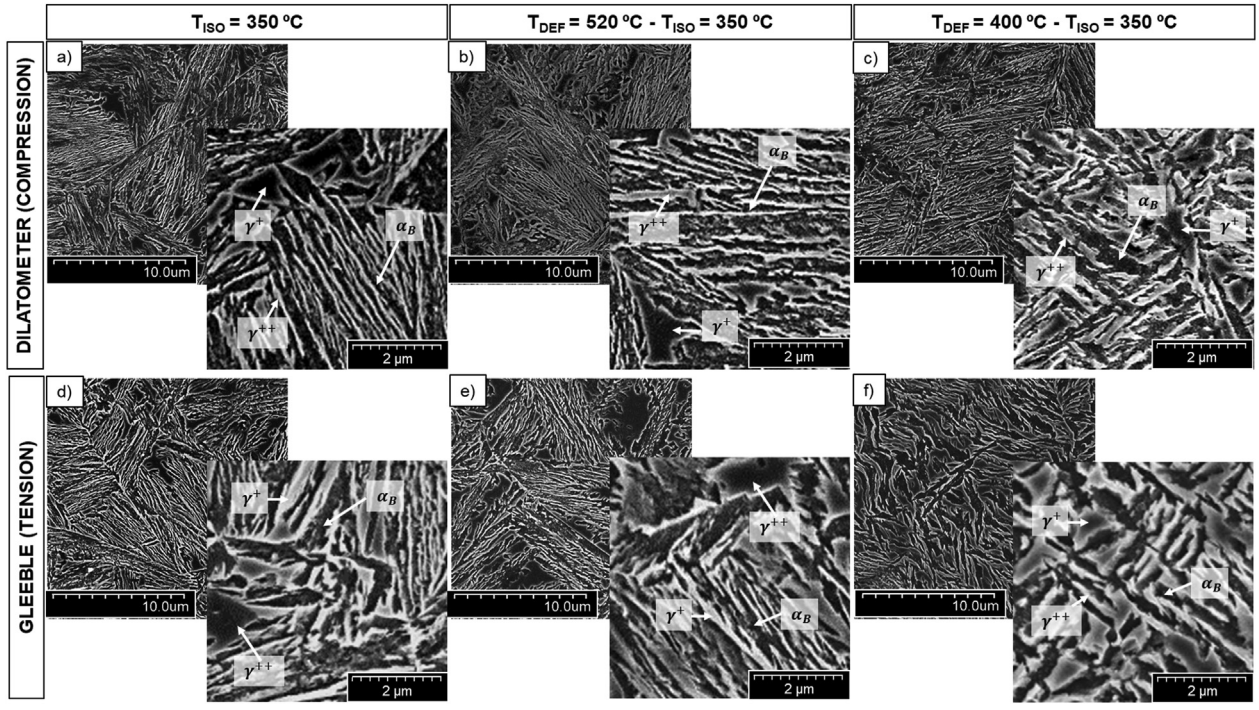

Fig. 6 – Intermediate and high magnification SEM micrographs corresponding to the T section of the samples subjected to (a, d) isothermal treatment at 350 °C; (b, e) ausforming treatment at 520 °C and (c, f) ausforming treatment at 400 °C in both the Bähr 805D dilatometer (a–c) and the Gleeble™ 3800 (d–f). The microstructural features characteristic of bainitic microstructures are indicated for each high magnification image.

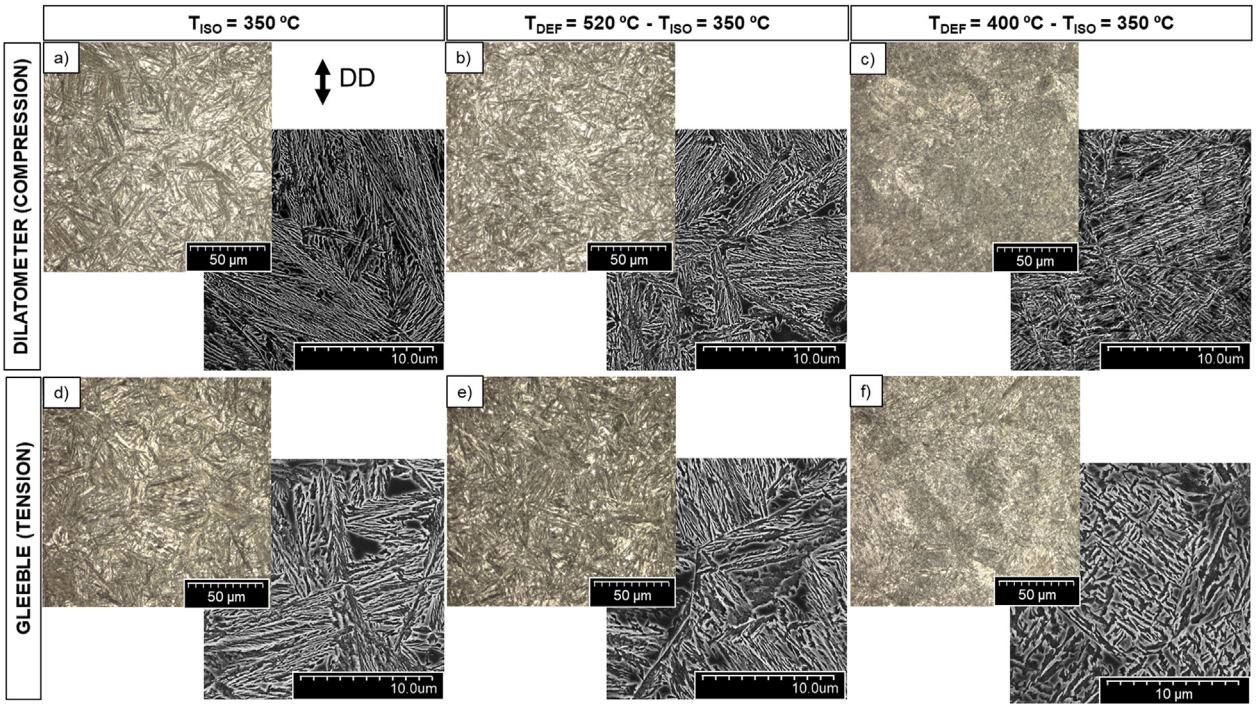

Fig. 7 – OM and SEM micrographs corresponding to the L section of the samples subjected to (a, d) an isothermal treatment at 350 °C; (b, e) an ausforming treatment at 520 °C and (c, f) an ausforming treatment at 400 °C in both the Bähr 805D dilatometer (a–c) and the Gleeble™ 3800 (d–f). The deformation direction (DD) is indicated on the top left.

micrographs corresponding to each of the studied conditions, respectively. While both figures includes SEM micrographs at intermediate magnification with the goal of depicting the microstructure, Fig. 6 also includes high magnification pictures of different features observed in the microstructure and Fig. 7 also includes low magnification OM micrographs that enable to observed the distribution of these features along the microstructures. For each condition, Table 3 includes the mean plate thicknesses measured on both T and L sections (t_T and t_L, respectively), together with their corresponding standard error. The volume fractions and crystallographic parameters, estimated from XRD patterns shown in Fig. 8, are included in Table 4. Finally, Table 5 includes the HRC values for all conditions and the equivalent HV values.

With respect to the isothermal treatments and their resultant microstructures, one can see that all microstructures are bainitic, consisting of bainitic ferrite plates, austenite blocks and thin films, as expected, see Fig. 6 (a, d) and Fig. 7 (a, d). Regarding the plate thickness, one can observe slight differences between the measurements made on the T and L sections, although they never exceed 9 nm, reason why these differences can be neglected. If one considers the values measured from both sections, it can be seen that there is a slight coarsening (max. 14 nm on L section) in the samples treated in the Gleeble™ 3800 thermomechanical simulator. The volume fractions, measured by XRD, do not significantly vary as a function of the equipment, as can be seen in Table 4. However, the dislocation density in bainitic ferrite and the crystallite size in thin film austenite show certain discrepancies. The microstructure processed in the Gleeble™ 3800 is also slightly softer, as can be seen in Table 5. These discrepancies could be associated to the fact that, when using the Gleeble™ 3800, the core was subjected to lower temperatures than the sample surface, which may mean that the isothermal treatment was not performed at 350 °C, but at a slightly higher temperature. Another possible reason is that the heating principle affects the bainitic transformation. Note that, in the past, an investigation showed that resistive heating affected some microstructural mechanisms, such as dislocation recovery, in a larger extent than conventional heating [22]. Although both heating systems of the Bähr 805D and the Gleeble™ 3800 are based on the Joule effect, their heating types are induction and resistance, respectively. To make sure that these slight changes do not affect the subsequent

Table 3 – Bainitic ferrite plate thickness measured on the T and L sections, respectively.

Condition	T_{ISO} = 350 °C		T_{DEF} = 520 °C -T_{ISO} = 350 °C		T_{DEF} = 400 °C -T_{ISO} = 350 °C	
Simulator	Bähr 805D	Gleeble™ 3800	Bähr 805D	Gleeble™ 3800	Bähr 805D	Gleeble™ 3800
t_T (nm)	91 ± 2	88 ± 2	84 ± 2	86 ± 2	88 ± 2	130 ± 3
t_L (nm)	82 ± 2	96 ± 2	70 ± 2	90 ± 2	87 ± 2	137 ± 3

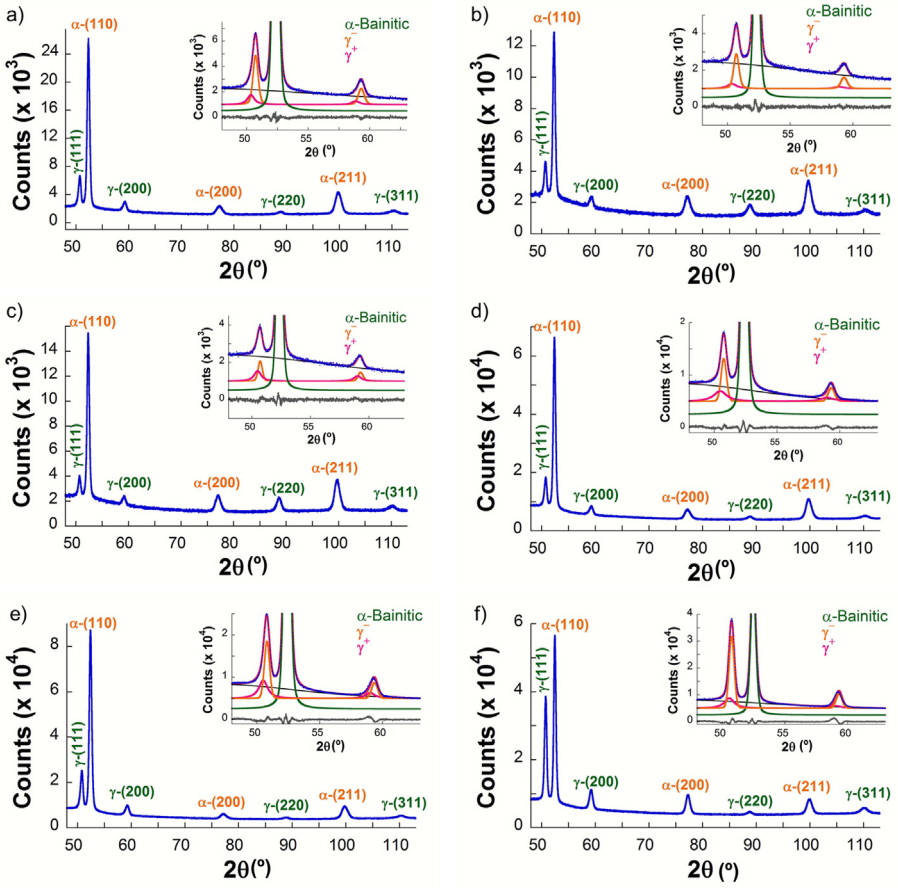

Fig. 8 – X-ray diffraction patterns and their corresponding Rietveld refinements corresponding to the samples subjected to (a, d) isothermal treatment at 350 °C; (b, e) ausforming treatment at 520 °C and (c, f) ausforming treatment at 400 °C in both the Bähr 805D dilatometer (a–c) and the Gleeble™ 3800 (d–f). In the Rietveld refinements, the contribution of the component phases is plotted in different colours (green for bainitic ferrite, orange for the blocky austenite (γ^-) and pink for the austenite thin films (γ^+), and the differences between experimental data and the fitted simulated pattern as a continuous grey line at the bottom

discussion, results were analysed in terms of differences between the ausforming conditions and the reference (isothermal) one.

The SEM study of the ausforming conditions - Fig. 6 (b, c, e, f) and Fig. 7 (b, c, e, f) also shows bainitic microstructures formed by bainitic ferrite plates, austenite blocks and thin films. Fig. 9

Table 4 – Crystallographic information corresponding to the bainitic ferrite (α_B), blocky austenite (γ^+) and austenite thin films (γ^{++}) for each tested condition , obtained by XRD. V and C stand for volume fraction and carbon content and ρ, λ and ε mean dislocation density, crystallite size and micro-strain.

Condition	T_{ISO} = 350 °C		T_{DEF} = 520 °C -T_{ISO} = 350 °C		T_{DEF} = 400 °C -T_{ISO} = 350 °C	
Simulator	Bähr 805D	Gleeble™ 3800	Bähr 805Dr	Gleeble™ 3800	Bähr 805D	Gleeble™ 3800
V_{α_B} (%)	81 ± 3	79 ± 3	76 ± 3	78 ± 3	73 ± 3	69 ± 3
V_{γ^+} (%)	14 ± 3	12 ± 3	19 ± 3	13 ± 3	13 ± 3	23 ± 3
$V_{\gamma^{++}}$ (%)	5 ± 3	9 ± 3	5 ± 3	9 ± 3	14 ± 3	8 ± 3
ρ_{α_B} (m^{-2})	$1.3\cdot10^{15} \pm 2\cdot10^{14}$	$8\cdot10^{14} \pm 1\cdot10^{14}$	$1.0\cdot10^{15} \pm 2\cdot10^{14}$	$9\cdot10^{14} \pm 1\cdot10^{14}$	$9\cdot10^{14} \pm 1\cdot10^{14}$	$7\cdot10^{14} \pm 1\cdot10^{14}$
C_{α_B} (wt. %)	0.16 ± 0.02	0.16 ± 0.02	0.16 ± 0.02	0.16 ± 0.02	0.16 ± 0.02	0.1 ± 0.02
λ_{α_B} (nm)	36 ± 2	49 ± 2	44 ± 2	51 ± 2	50 ± 2	59 ± 2
ε_{α_B}	0.0018 ± 0.0002	0.0016 ± 0.0002	0.0017 ± 0.0002	0.0017 ± 0.0002	0.0017 ± 0.0002	0.0016 ± 0.0002
C_{γ^+} (wt. %)	0.99 ± 0.03	1.08 ± 0.03	0.97 ± 0.03	1.05 ± 0.03	1.07 ± 0.03	1.23 ± 0.03
λ_{γ^+} (nm)	>150	>150	>150	>150	>150	>150
ε_{γ^+}	0.002 ± 0.0002	0.0021 ± 0.0002	0.0021 ± 0.0002	0.002 ± 0.0002	0.0017 ± 0.0002	0.002 ± 0.0002
$C_{\gamma^{++}}$ (wt. %)	1.76 ± 0.03	1.66 ± 0.03	1.65 ± 0.03	1.65 ± 0.03	1.51 ± 0.03	1.62 ± 0.03
$\lambda_{\gamma^{++}}$ (nm)	12 ± 2	6 ± 2	9 ± 2	9 ± 2	11 ± 2	8 ± 2
$\varepsilon_{\gamma^{++}}$	–	–	–	–	–	–

Table 5 – Hardness measurements made on the T section of the sample center.

Condition	$T_{ISO} = 350$ °C		$T_{DEF} = 520$ °C -$T_{ISO} = 350$ °C		$T_{DEF} = 400$ °C -$T_{ISO} = 350$ °C	
Simulator	Bähr 805D	Gleeble™ 3800	Bähr 805D	Gleeble™ 3800	Bähr 805D	Gleeble™ 3800
HRC	45.4 ± 0.4	43.7 ± 0.7	43.5 ± 1.0	42.7 ± 0.7	42.6 ± 0.4	38.5 ± 1.1
HV	493 ± 1	488 ± 4	484 ± 6	481 ± 9	478 ± 2	428 ± 1

includes bar charts representing the plate thickness increase, measured on the T and L sections. All increases are calculated with respect to their corresponding values for the isothermal condition (for the same equipment). In terms of plate thickness, ausforming at 520 °C leads to a very slight refinement, regardless of the deformation mode, as can be observed in Fig. 9 (a, b). The most evident increase in plate thickness is found for the sample ausformed at 400 °C under tensile conditions, regardless of the section of measurement, see Fig. 9 (a, b). The reason of this coarsening is most likely the presence of strain induced bainitic ferrite formed at $\geq$ 400 °C, as previously discussed. For the treatment with $T_{DEF} = 400$ °C under compression, while a coarsening is observed for the L section, a refinement is detected on the T section. This behavior could be most likely due to the previously discussed variant selection phenomenon, that leads to anisotropic microstructures in which the methodology to estimate plate thickness is no longer accurate as its stereographic correction assumes that bainitic ferrite plates are randomly distributed [30]. Thus, the methodology can only be useful to roughly estimate whether a treatment leads to significant refinement or coarsening [8].

With respect to the distribution of the bainitic ferrite plates, it can be observed that, when a compressive deformation was applied, especially at 400 °C, bainitic ferrite plates were highly aligned on the L section (Fig. 7(c)), as also previously reported in similar structures [8]. This behavior was also found for the microstructures subjected to tension, as can be seen in Fig. 7(f). Moreover, the angles between the plates and the DD were measured and their histograms are shown in Fig. 10, where it can be observed that they varied depending on the applied thermomechanical conditions. These changes could be associated to the macro-texture of the prior austenite, which changes depending on the deformation mode [31]. Such a texture change is expected to affect the value of the Schmid factor for each of the slip systems of the prior austenite grains, as has been previously proved in stainless steels [28]. Hence, the orientation of the deformation micro-bands is expected to change too, which finally affects the orientation of the formed bainitic ferrite and, thus, the displacement gradient tensor associated to the bainitic transformation, whose third principal component is the relative change in length along the Z-axis [7].

To try to understand the obtained results, the angles between the austenite microbands, along which plates are expected to be formed, and the DD were theoretically calculated. For the calculations, it was assumed that the austenite texture was characterized by the <010> and the <011> families of directions parallel to the DD when the deformation mode was compression and by the <010> and the <111> families of directions parallel to the DD when the deformation mode was tension [32]. The theoretical values are also included in Fig. 10. It is important to emphasize that the samples ausformed at 400 °C were also subjected to strain induced transformations, mainly controlled by the applied stress, i.e. by ΔG_{mech} [15]. The angles between the plates and the DD that would lead to the maximum ΔG_{mech} are also included in Fig. 10. These values were obtained based on the relation proposed by Patel and Cohen [29], i.e. $\Delta G_{mech} = -\frac{1}{2}s\sigma \sin 2\theta \pm \frac{1}{2}\zeta\sigma(1+\cos 2\theta)$, where the second term is preceded by a plus sign in the case the deformation mode is compression and a minus sign in the case the deformation mode is tension [29] and where s and ζ are the shear and dilatational strains associated transformation, which were taken as 0.26 and 0.03, respectively [33]. The angle θ was considered as the angle for which the transformation was promoted the most (i.e. ΔG_{mech} was

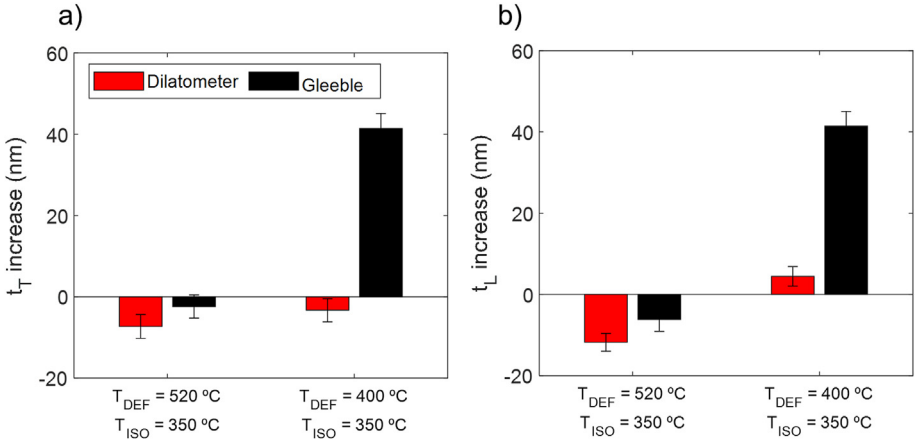

Fig. 9 – Comparison between increase in bainitic ferrite plate thickness measured on the T (a) and L (b) sections for ausforming, as compared to the bainitic ferrite plate thickness corresponding to the isothermal conditions.

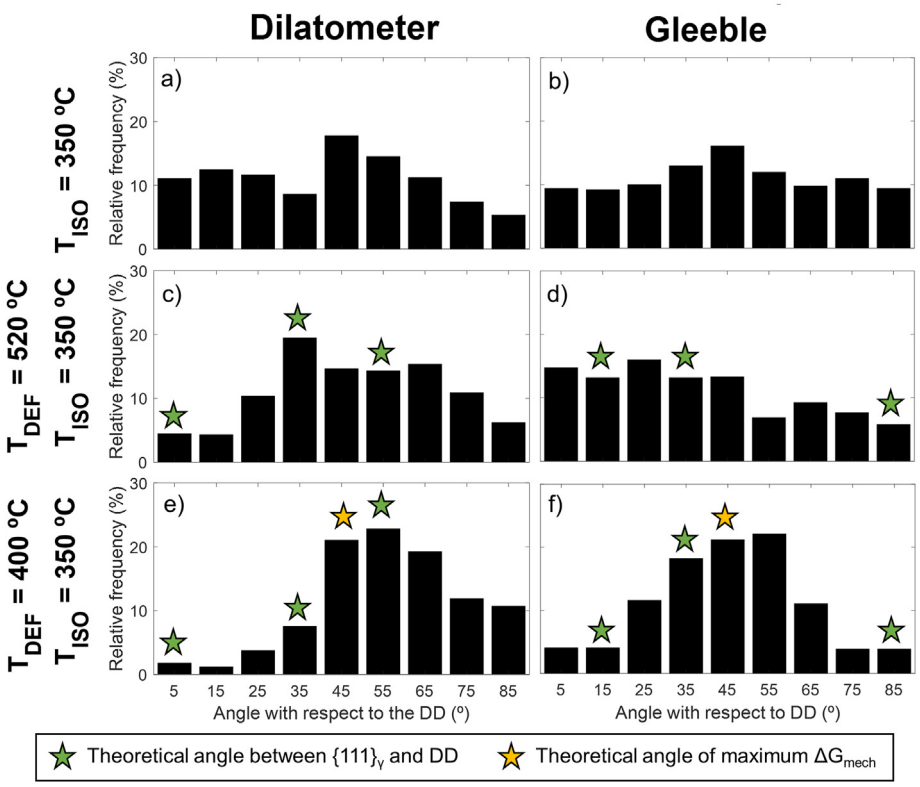

Fig. 10 – For the six conditions of study, histograms of the angles between the bainitic ferrite plates and the DD. The theoretical angles that would correspond to plates lying along deformation microbands {111} and to plates grown to maximize ΔG_{mech} are also included.

maximum in absolute value): $\theta = \arctan\left(\frac{s}{\zeta}\right)/2$ [29]. As can be observed, the experimental results cannot be explained based on these theoretical calculations, which indicates that this methodology cannot be applied to very fine bainitic microstructures, where the error associated to the manual measurement is too high.

Finally, Fig. 11 includes bar charts representing increase in several parameters, as compared to the reference: the XRD volume percentages of the different phases, the carbon content of those given phases, the dislocation density of the bainitic ferrite and the microstructure HRC. Fig. 11 (a) shows that, regardless of the deformation mode, the volume fraction of bainitic ferrite decreases for lower T_{DEF}, in agreement with previously reported results in the literature [4]. As shown in Table 4 and Fig. 11(b), the carbon content of the bainitic ferrite remains constant, taking a value of 0.16 wt. % for all conditions except for the one subjected to ausforming at 400 °C in the Gleeble™ 3800. This behavior can be understood by considering that the material underwent a strain induced bainitic transformation above 400 °C and that the carbon content of bainitic ferrite has been reported to decrease as T_{ISO} increases [17,34,35]. With respect to the dislocation density in bainitic ferrite, included in Fig. 11(c), one can see that it decreased for the ausforming conditions, especially when the deformation mode was compression. This decrease is mainly associated to the variation of crystallite size, as micro-strain remains constant for all conditions, as can be observed in Table 4. One possible reason of this behaviour could be the effect of the heating principle on the recovery of dislocations, as previously discussed for the isothermal conditions.

Regarding the retained austenite present in the microstructure, XRD results confirmed that ausforming at 520 °C did not lead to notable variations of blocky and thin film austenite volume fractions, considering the associated error, see Fig. 11(d, e). However, samples ausformed at 400 °C did present variations, although their extent changed with the deformation mode. Samples subjected to compression ausforming presented an increased volume fraction of thin film austenite - Fig. 11 (e) -, in good agreement with previous works from the literature that link the phenomenon to variant selection [36–38]. Nevertheless, samples subjected to tensile ausforming presented a higher volume fraction of blocky austenite, as can be seen in Fig. 11(d). This discrepancy could be associated to the more chaotic dynamic phase transformation happening for this condition. A higher fraction of blocky austenite could deteriorate the microstructure mechanical properties, as blocky austenite is more prone to go through transformation induced plasticity (TRIP) effect than thin film austenite [39–41].

With respect to carbon content of both morphologies of retained austenite, see Fig. 11(f, g), it is clear that ausforming decreases the carbon content in thin film austenite, where this effect is more pronounced for lower deformation temperatures and, specially, for compression ausforming,

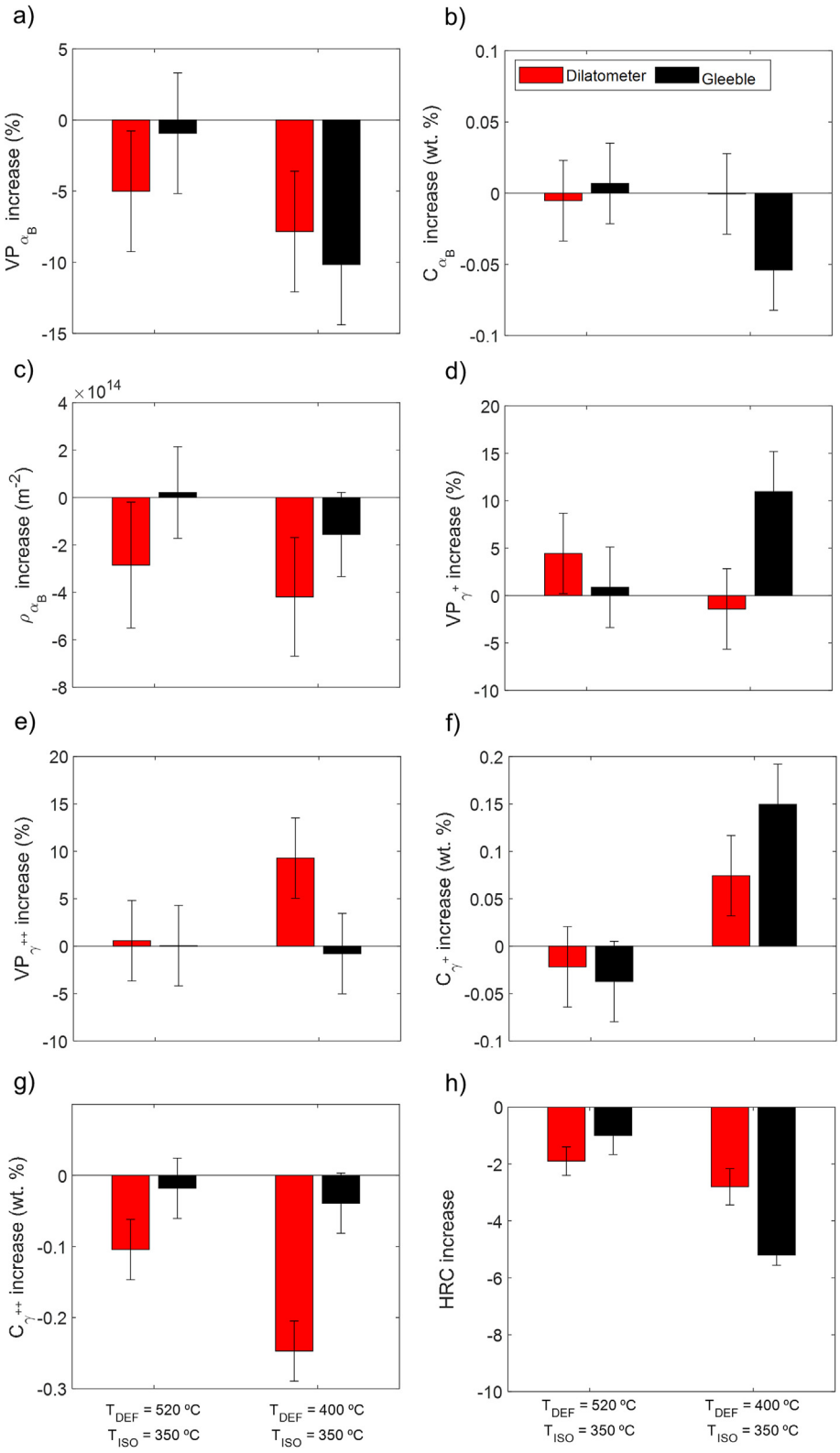

Fig. 11 – Comparison between increase in different parameters obtained in the ausformed samples, as compared to the isothermal condition. These parameters are: (a, b, c) volume fraction, carbon content and dislocation density of bainitic ferrite, respectively; (d, e) volume fractions of blocky and thin film austenite, respectively; (f, g) carbon content of blocky and thin film austenite, respectively and (h) HRC.

Fig. 11(g). The effect of deformation on the variations of the carbon content of blocky austenite is not so clear. For instance, samples ausformed at 520 °C present lower carbon contents than the reference isothermal sample, while the opposite is true for the samples ausformed at 400 °C, as can be observed in Fig. 11(f). In contrast, the crystallite size and the microstrain of the blocky and thin film austenite remained almost constant as a function of the deformation mode, as shown in Table 4.

Finally, it is clear from Fig. 11(h) that ausforming slightly decreases hardness for all conditions, although the hardness reduction is only significant when strain induced transformations take place during the process.

4. Conclusions

Different conclusions were drawn from this work:

(1) The deformation mode affected the anisotropy shown by the microstructures subjected to ausforming in a different way: the dilatometric signals were different and the structures presented bainitic ferrite plates that were differently aligned with respect to the DD depending on the deformation mode.
(2) Ausforming at 400 °C was characterized by leading to strain induced bainitic transformations during the deformation step, especially intense for tensile ausforming. The presence of bainitic ferrite dynamically formed during the deformation step at high temperature led to microstructural coarsening that was not detected otherwise.
(3) As the deformation temperatures decreased, so did the volume fractions of bainitic ferrite, regardless of the deformation mode. However, the increase in retained austenite for the lowest deformation temperature did not always lead to the reduction of the same morphology of retained austenite.
(4) The carbon content of bainitic ferrite was constant, regardless of the condition, except when a very high fraction of strain induced bainitic ferrite formed – tensile ausforming at 400 °C. Both the deformation temperature and the deformation mode affected the carbon content of blocky austenite and thin film austenite.
(5) Significant hardness variations are only detected when strain induced transformations happen during the process – ausforming at 400 °C. Therefore, when designing an industrial ausforming process, it is suggested to pay special attention to these dynamic transformations, that can impair the microstructure properties very notably.

Declaration of Competing Interest

The authors declare that they have no known competing financial interests or personal relationships that could have appeared to influence the work reported in this paper.

Acknowledgments

The authors gratefully acknowledge the support for this work by the European Research Fund for Coal and Steel under the Contract RFCS-2015-709607. The authors also acknowledge the supports of the Metallography and Phase Transformations, the X-Ray and the Microscopy laboratories at CENIM. Adriana Eres-Castellanos acknowledges the Fonds de recherche du Québec – Nature et technologies (FRQNT) for the support received under the Merit scholarship program for foreign students, personal ref 290835.

REFERENCES

[1] Gong W, Tomota Y, Koo MS, Adachi Y. Effect of ausforming on nanobainite steel. Scr Mater 2010;63:819–22. https://doi.org/10.1016/j.scriptamat.2010.06.024.
[2] Garcia-Mateo C, Eres-Castellanos A, Caballero FG, Lazt A, Schreiber S, Ray A, et al. Towards industrial applicability of (medium C) nanostructured bainitic steels (TIANOBAIN). 2020.
[3] Zhang M, Wang YH, Zheng CL, Zhang FC, Wang TS. Effects of ausforming on isothermal bainite transformation behaviour and microstructural refinement in medium-carbon Si-Al-rich alloy steel. Mater Des 2014;62:168–74. https://doi.org/10.1016/j.matdes.2014.05.024.
[4] Shipway PH, Bhadeshia HKDH. Mechanical stabilisation of bainite. Mater Sci Technol 1995;11:1116–28.
[5] Chatterjee S, Wang HS, Yang JR, Bhadeshia HKDH. Mechanical stabilisation of austenite. Mater Sci Technol 2006;22:641–4.
[6] Gong W, Tomota Y, Adachi Y, Paradowska AM, Kelleher JF, Zhang SY. Effects of ausforming temperature on bainite transformation, microstructure and variant selection in nanobainite steel. Acta Mater 2013;61:4142–54. https://doi.org/10.1016/j.actamat.2013.03.041.
[7] Eres-Castellanos A, Morales-Rivas L, Caballero FG, Garcia-Mateo C. Explaining the dilatometric behavior during bainite transformation under the effect of variant selection. J Alloys Compd 2021;864:158130.
[8] Eres-Castellanos A, Morales-Rivas L, Latz A, Caballero FG, Garcia-Mateo C. Effect of ausforming on the anisotropy of low temperature bainitic transformation. Mater Char 2018;145:371–80. https://doi.org/10.1016/j.matchar.2018.08.062.
[9] Eres-Castellanos A, Hidalgo J, Morales-Rivas L, Caballero FG, Garcia-Mateo C. The role of plastic strains on variant selection in ausformed bainitic microstructures studied by finite elements and crystal plasticity simulations. J Mater Res Technol 2021;13:1416–30.
[10] Zorgani M, Garcia-Mateo C, Jahazi M. The role of ausforming in the stability of retained austenite in a medium-C carbide-free bainitic steel. J Mater Res Technol 2020;9:7762–76.
[11] Hu H, Xu G, Wang L, Zhou M. Effects of strain and deformation temperature on bainitic transformation in a Fe-C-Mn-Si alloy. Steel Res Int 2016;88(3):1600170–7. https://doi.org/10.1002/srin.201600170.
[12] Chen SP, Rana R, Xiao B, Haldar A. The effects of hot deformation of austenite on the bainite transformation in a Fe-C-Mn-Si-Cr steel. Mater Sci Forum 2018;941:486–91. Trans Tech Publ.

[13] Bhalla G, Tsang MH, Gao D, Chen Q, Ruhe W, Ushioda N. Frictional properties of molybdenum-based lubricating oil additives using green chemistry. SAE Int J Fuels Lubr 2012;5:496–503.
[14] Soliman M, Ibrahim H, Nofal A, Palkowski H. Effect of intercritical annealing on phase transformation and mechanical properties of thermo-mechanically processed dual matrix ductile iron. In: TMS 2014 143rd annu. Meet. Exhib. Springer; 2014. p. 959–65.
[15] Eres-Castellanos A, Caballero FG, Garcia-Mateo C. Stress or strain induced martensitic and bainitic transformations during ausforming processes. Acta Mater 2020;189:60–72. https://doi.org/10.1016/j.actamat.2020.03.002.
[16] Garcia-Mateo C, Jimenez JA, Lopez-Ezquerra B, Rementeria R, Morales-Rivas L, Kuntz M, et al. Analyzing the scale of the bainitic ferrite plates by XRD, SEM and TEM. Mater Char 2016;122:83–9. https://doi.org/10.1016/j.matchar.2016.10.023.
[17] Garcia-Mateo C, Jimenez JA, Yen HW, Miller MK, Morales-Rivas L, Kuntz M, et al. Low temperature bainitic ferrite: evidence of carbon super-saturation and tetragonality. Acta Mater 2015;91:162–73. https://doi.org/10.1016/j.actamat.2015.03.018.
[18] Dyson DJ, Holmes B. Effect of alloying additions on lattice parameter of austenite. J Iron Steel Inst 1970;208:469–74.
[19] Cohen M. Strengthening of steel. 1962. 1962.
[20] Williamson GK, Smallman III RE. Dislocation densities in some annealed and cold-worked metals from measurements on the X-ray debye-scherrer spectrum. Philos Mag 1956;1:34–46. https://doi.org/10.1080/14786435608238074.
[21] Bachmann F, Hielscher R, Schaeben H. Texture analysis with MTEX–free and open source software toolbox. Solid State Phenom 2010;160:63–8. Trans Tech Publ.
[22] Nicolaÿ A, Franchet J-M, Cormier J, Logé RE, Fiorucci G, Fausty J, et al. Influence of Joule effect heating on recrystallization phenomena in inconel 718. Metall Mater Trans A 2021;52:4572–96.
[23] Eres-Castellanos A, Morales-Rivas L, Jimenez JA, Caballero FG, Garcia-Mateo C. Effect of ausforming on the macro and micro-texture of bainitic microstructures. Metallurgical and Materials Transactions A 2021;52:4033–52.
[24] Bhadeshia HKDH, David SA, Vitek JM, Reed RW. Stress induced transformation to bainite in Fe-Cr-Mo-C pressure vessel steel. Mater Sci Technol 1991;7:686–98. https://doi.org/10.1179/mst.1991.7.8.686.
[25] Umemoto M, Bando S, Tamura I. Morphology and transformation kinetics of bainite in Fe-Ni-C and Fe-Ni-Cr-C alloys. In: Proc. Int. Conf. Martensitic transform. (ICOMAT-86), August 26-30, 1986; 1986. p. 595–600. Nara, Japan.
[26] Zhou M, Xu G, Zhang Y, Xue Z. The effects of external compressive stress on the kinetics of low temperature bainitic transformation and microstructure in a superbainite steel. Int J Mater Res 2015;106:1040–5. https://doi.org/10.3139/146.111274.
[27] Brunelli K, Bassani P, Lecis N, Peruzzo L, Maranzana C, Dabala M. Microstructural evolution of a continuously cooled air hardening steel. Metallogr Microstruct Anal 2013;2:56–66.
[28] El-Tahawy M, Jenei P, Kolonits T, Han G, Park H, Choe H, et al. Different evolutions of the microstructure, texture, and mechanical performance during tension and compression of 316L stainless steel. Metall Mater Trans A 2020;51:3447–60.
[29] Patel JR, Cohen M. Criterion for the action of applied stress in the martensitic transformation. Acta Metall 1953;1:531–8. https://doi.org/10.1016/0001-6160(53)90083-2.
[30] Mack C, Bartlett MS. On clumps formed when convex laminae or bodies are placed at random in two or three dimensions. Math Proc Camb Phil Soc 1956;52:246–50. https://doi.org/10.1017/S0305004100031236.
[31] Hosford WF. Slip and Crystallographic Textures. Mechanical Behavior of Materials. Cambridge University Press; 2009. p. 113–36.
[32] Wroński M, Wierzbanowski K. Lattice rotation definition and predicted textures of tensile and compression deformation. Arch Metall Mater 2016;61(3):1529–36.
[33] Swallow E, Bhadeshia HKDH. High resolution observations of displacements caused by bainitic transformation. Mater Sci Technol 1996;12:121–5.
[34] Bhadeshia HKDH. Bainite in steels: theory and practice. Boca Raton, FL, USA: CRC Press; 2019.
[35] Garcia-Mateo C, Caballero FG, Bhadeshia HKDH. Development of hard bainite. ISIJ Int 2003;43:1238–43. https://doi.org/10.2355/isijinternational.43.1238.
[36] Fan H, Zhao A, Li Q, Guo H, He JG. Effects of ausforming strain on bainite transformation in nanostructured bainite steel. Int J Miner Metall Mater 2017;24:264–70.
[37] Hu H, Xu G, Wang L, Zhou MX, Xue ZL. Effect of ausforming on the stability of retained austenite in a C-Mn-Si bainitic steel. Met Mater Int 2015;21:929–35. https://doi.org/10.1007/s12540-015-5156-5.
[38] Golchin S, Avishan B, Yazdani S. Effect of 10% ausforming on impact toughness of nano bainite austempered at 300°C. Mater Sci Eng A 2016;656:94–101. https://doi.org/10.1016/j.msea.2016.01.025.
[39] Garcia-Mateo C, Caballero FG. The role of retained austenite on tensile properties of steels with bainitic microstructures. Mater Trans 2005;46:1839–46. https://doi.org/10.2320/matertrans.46.1839.
[40] Avishan B, Garcia-Mateo C, Morales-Rivas L, Yazdani S, Caballero FG. Strengthening and mechanical stability mechanisms in nanostructured bainite. J Mater Sci 2013;48:6121–32. https://doi.org/10.1007/s10853-013-7408-4.
[41] Xiong XC, Chen B, Huang MX, Wang JF, Wang L. The effect of morphology on the stability of retained austenite in a quenched and partitioned steel. Scr Mater 2013;68:321–4. https://doi.org/10.1016/j.scriptamat.2012.11.003.